

# THE PLASMON IN HOT $\phi^4$ THEORY

Enke Wang\* and Ulrich Heinz

*Institut für Theoretische Physik, Universität Regensburg,*

*D-93040 Regensburg, Germany*

(September 26, 2021)

## Abstract

We study the 2-loop resummed propagator in hot  $g^2\phi^4$  theory. The propagator has a cut along the whole real axis in the complex energy plane, but for small  $g$ , the spectral density is sharply peaked around the plasmon. The dispersion relation and the width of the plasmon are calculated at zero *and* finite momentum. At large momenta the spectral width vanishes, and the plasmon loses its collectivity and behaves like a non-interacting free particle.

PACS numbers: 12.38Cy, 12.38Bx, 11.10Wx, 12.38Mh

## I. INTRODUCTION

At high temperature  $T$  and low momenta  $p < T$  the effective degrees of freedom in any field theory are collective modes, bosonic “plasmons” [1,2] and fermionic “plasminos” [3,4]. Even if the fundamental field theoretical degrees of freedom were massless, the collective modes possess a finite “thermal” mass which is generated dynamically by the interactions among the fundamental degrees of freedom. The thermal masses regulate (some of) the severe infrared divergences which the massless theory would otherwise develop at finite temperature due to the singularity of the Bose distribution at zero momentum [5,6]. The strong rise of the Bose distribution at small momenta causes, for example, the transport properties (viscosity, heat conduction) of a hot plasma of massless fields to be dominated by the interaction between low-momentum collective modes [7,8]. The determination of their dispersion relation and their collisional width is therefore a necessary prerequisite for any microscopic calculation of the transport coefficients, for example using the Kubo formulae [9].

It is known that a consistent determination of the plasmon dispersion relation and width in a massless field theory requires the resummation of certain loop contributions to the propagator, the so-called “hard thermal loops” (HTL) [6]. In massless gauge theories, this resummation becomes non-trivial beyond leading order, due to the complicated analytical structure of the HTLs (i.e. their momentum dependence and logarithmic branch cuts from Landau damping [1,2]). In massless scalar  $\phi^4$  theory, the resummation is much easier [10,5], since the leading HTL (the tadpole diagram) is just a momentum-independent real constant, and it can therefore be relatively easily be carried beyond leading order [11]. Still, when we started this work, no calculation of the collisional *width* of finite momentum plasmons existed. Since the latter is needed, however, for the calculation of transport coefficients from the Kubo formulae (previous calculations [8,13] used, for lack of better knowledge but without justification, the zero momentum limit of the plasmon width), we present in this paper a calculation of the resummed scalar field propagator in  $g^2\phi^4$  theory at the 2-loop

level, including real *and* imaginary parts in 4-dimensional momentum space. While this work was in progress, Jeon [12] presented a calculation of the plasmon width at zero and finite momentum on the plasmon mass shell. Our results agree with his and extend them into the off-shell domain.

This paper is organized as follows. In Section II we will give a brief review of results from Ref. [11] on resummation in hot  $\phi^4$  theory which we will need later. In Section III we present the calculation of the imaginary part of the 2-loop self-energy and investigate the analytical structure of the full propagator at two-loop order. The properties of plasmons at rest and at finite momentum are studied analytically and numerically in Sections III A and III B, respectively. Our conclusions are summarized in Section IV. Appendix A contains some technical steps of the calculations in Section III.

## II. RESUMMATION AT HIGH TEMPERATURE

For a hot scalar field, we consider the following Lagrangian with  $\lambda = \frac{g^2}{4!} < 1$ :

$$\mathcal{L}_0 = \frac{1}{2}(\partial_\mu\phi)^2 + \frac{g^2}{4!}\phi^4. \quad (2.1)$$

At the tree level it describes massless scalar fields with a quartic self interaction. The induced thermal mass resulting from the single HTL (tadpole) is of order  $g$  and reads [10,11]

$$m_{\text{th}}^2 = \frac{g^2 T^2}{24}. \quad (2.2)$$

The effects from this thermal mass can be resummed by defining an effective Lagrangian through

$$\mathcal{L} = \left(\mathcal{L}_0 + \frac{1}{2}m_{\text{th}}^2\phi^2\right) - \frac{1}{2}m_{\text{th}}^2\phi^2 = \mathcal{L}_{\text{eff}} - \frac{1}{2}m_{\text{th}}^2\phi^2, \quad (2.3)$$

and treating the last term as an additional interaction. This effective Lagrangian defines an effective propagator with thermal mass  $m_{\text{th}}$

$$\Delta = \frac{1}{K^2 + m_{\text{th}}^2}, \quad (2.4)$$

where in the imaginary time formalism  $K^2 = k_0^2 + \mathbf{k}^2$ ,  $k_0 = 2n\pi T$ ,  $n = 0, \pm 1, \pm 2, \dots$ . It represents the infinite sum of iterated HTLs. Since  $m_{\text{th}}$  leads to a qualitative modification of the resummed effective propagator for soft momenta,  $p \leq gT$ , its inclusion via resummation is necessary to avoid infrared divergences at finite temperature [5]. Vertex corrections from HTLs are down by a factor  $g$  relative to the bare vertex  $g^2$  and don't qualitatively change the latter. In a perturbative expansion of  $\phi^4$  theory we can thus keep using the bare vertex [11].

One can now recalculate the 1-loop self-energy using this resummed effective propagator. This amounts to computing the contribution of all “cactus diagrams” or “superdaisies” in the original Lagrangian [10] each of which is infrared divergent. Using dimensional regularization in the MS renormalization scheme, the diagram in Fig. 1a gives

$$\Sigma'_1 = \frac{g^2 T^2}{24} \left( -1 + \frac{3m_{\text{th}}}{\pi T} + \frac{3}{4\pi^2} \left( \frac{m_{\text{th}}}{T} \right)^2 \left[ \ln \left( \frac{\mu^2}{4\pi T^2} \right) + \gamma_E \right] \right) + \mathcal{O}(g^5 \ln g), \quad (2.5)$$

where  $\mu$  is the scale parameter in dimensional regularization and  $\gamma_E = 0.577216\dots$  is Euler's constant. The resummation of an infinite series of infrared diagrams reflects itself through a  $g^3$  correction to the leading term  $-g^2 T^2 / 24 = -m_{\text{th}}^2$ ; it is non-analytic in the coupling constant  $\lambda = g^2 / 24$  and for  $g \ll 1$  dominates any finite genuinely perturbative corrections of order  $g^4$ . In this sense resummation is essential.

Including also the contribution from the new 2-point interaction in (2.3), Fig. 1b, the full 1-loop self-energy can be written as  $\Sigma_1 = \Sigma'_1 + m_{\text{th}}^2$ . It is purely real. Thus, to order  $g^3$ , the full propagator has only two poles at  $p_0 = \pm \sqrt{\mathbf{p}^2 + m_p^2}$  where  $m_p$  is the 1-loop resummed plasmon mass:

$$m_p = m_{\text{th}} \sqrt{1 - \frac{3m_{\text{th}}}{\pi T}}. \quad (2.6)$$

Following Ref. [11], we can now improve the resummation procedure by including into the effective Lagrangian all 1-loop effects which are independent of the regularization scheme, i.e. by writing

$$\mathcal{L} = \left( \mathcal{L}_0 + \frac{1}{2} m_p^2 \phi^2 \right) - \frac{1}{2} m_p^2 \phi^2 \quad (2.7)$$

and expanding into effective scalar propagators with an effective plasmon mass  $m_p$ . Then all factors  $m_{\text{th}}$  in Eq. (2.5) are replaced by  $m_p$ , and from the full 1-loop self energy  $\Sigma_1 = \Sigma'_1 + m_p^2$  all terms up to order  $g^3$  cancel, leaving a leading contribution of order  $g^4$  which is real.

At 2-loop order, the Feynman diagrams shown in Fig. 2 contribute. Their leading contributions are also of order  $g^4$ . Diagram 2c arises from the new 2-point interaction of the Lagrangian (2.7) and contributes at the same order.

The contribution  $\Sigma'_2$  of the diagrams 2a and 2c is easily evaluated. It is purely real. As a consequence of resummation, all leading  $g^4$  terms cancel, and the result is found to be

$$\Sigma'_2 = \mathcal{O}(g^5 \ln g). \quad (2.8)$$

A convenient way to calculate diagram 2b is to use the Saclay method [14]. Its contribution can be expressed as

$$\begin{aligned} \Sigma''_2(ip_0, \mathbf{p}) = & \int d[k, q] \left\{ S(E_k, E_q, E_r)[(1 + f_k)(1 + f_q)(1 + f_r) - f_k f_q f_r] \right. \\ & + S(E_k, E_q, -E_r)[(1 + f_k)(1 + f_q)f_r - f_k f_q(1 + f_r)] \\ & + S(E_k, -E_q, E_r)[(1 + f_k)f_q(1 + f_r) - f_k(1 + f_q)f_r] \\ & \left. + S(-E_k, E_q, E_r)[f_k(1 + f_q)(1 + f_r) - (1 + f_k)f_q f_r] \right\}, \end{aligned} \quad (2.9)$$

with the same notation as in Ref. [11], namely

$$d[k, q] = \frac{g^4 \mu^{4\varepsilon}}{6} \frac{d^{D-1}k}{(2\pi)^{D-1}} \frac{d^{D-1}q}{(2\pi)^{D-1}} \frac{1}{8E_k E_q E_r}, \quad (2.10)$$

$$S(E_k, E_q, E_r) = \frac{1}{ip_0 + E_k + E_q + E_r} - \frac{1}{ip_0 - E_k - E_q - E_r}, \quad (2.11)$$

where

$$r = |\mathbf{k} + \mathbf{q} - \mathbf{p}|, \quad (2.12)$$

$$E_l^2 = l^2 + m_p^2, \quad l = k, q, r, \quad (2.13)$$

$$f_l = \frac{1}{\exp(E_l/T) - 1}, \quad l = k, q, r. \quad (2.14)$$

$D = 4 - 2\varepsilon$  is the the number of space-time dimension introduced in dimensional regularization. Please notice that now the one-loop resummed mass  $m_p$  occurs in all on-shell

energies. The real part of  $\Sigma_2''$  contains an ultraviolet divergence. A detailed discussion of the subtraction of this ultraviolet divergence by a counter-term in the Lagrangian and the final expression for the real part of the renormalized self-energy can be found in Ref. [11]. We can see from Eq. (2.10) that  $\text{Re } \Sigma_2''$  is of the order  $g^4$  and depends on the mass parameter  $\mu$  of the dimensional regularization.

The complete 2-loop expression for the real part of the self-energy is given by

$$\text{Re } \Sigma(ip_0, \mathbf{p}) = \Sigma_1 + \Sigma_2' + \text{Re } \Sigma_2''(ip_0, \mathbf{p}), \quad (2.15)$$

with the last term taken from Ref. [11]. A detailed calculation of the imaginary part of the self-energy will be given in the following section.

### III. FULL PROPAGATOR AND SPECTRAL FUNCTION OF THE PLASMON

The leading contribution to the imaginary part of the self energy comes from the 2-loop diagram 2b. Making an analytical continuation  $ip_0 = \omega + i\eta$ ,  $\eta = 0^+$ , and using  $1/(A + i\eta) = \mathcal{P}(1/A) - i\pi\delta(A)$ , we obtain from Eq. (2.9)

$$\begin{aligned} \text{Im } \Sigma(\omega, \mathbf{p}) = \text{Im } \Sigma_2''(\omega, \mathbf{p}) &= -\pi \int d[k, q] \quad (3.1) \\ &\left\{ [\delta(\omega + E_k + E_q + E_r) - \delta(\omega - E_k - E_q - E_r)][(1 + f_k)(1 + f_q)(1 + f_r) - f_k f_q f_r] \right. \\ &+ [\delta(\omega + E_k + E_q - E_r) - \delta(\omega - E_k - E_q + E_r)][(1 + f_k)(1 + f_q)f_r - f_k f_q(1 + f_r)] \\ &+ [\delta(\omega + E_k - E_q + E_r) - \delta(\omega - E_k + E_q - E_r)][(1 + f_k)f_q(1 + f_r) - f_k(1 + f_q)f_r] \\ &\left. + [\delta(\omega - E_k + E_q + E_r) - \delta(\omega + E_k - E_q - E_r)][f_k(1 + f_q)(1 + f_r) - (1 + f_k)f_q f_r] \right\}. \end{aligned}$$

This gives the rates for physical decay and scattering processes [15]: The first line corresponds to the decay of one off-shell into three on-shell  $\phi$  mesons and (with opposite sign) the inverse process; the two  $\delta$ -functions represent the decay of particles with negative and positive energy, respectively. The remaining lines in Eq. (3.1) correspond to Landau damping via scattering of the off-shell meson with on-shell particles from the heat bath, forward and backward scattering process contributing with opposite signs. Landau damping requires the

presence of thermally excited states and vanishes at zero temperature. In each term every ingoing meson from the heat bath receives a thermal weight  $f_i$  and each outgoing one a Bose-enhancement factor  $(1 + f_i)$ .

It is easy to show that

$$\text{Re } \Sigma(-\omega, \mathbf{p}) = \text{Re } \Sigma(\omega, \mathbf{p}) \quad \text{and} \quad \text{Im } \Sigma(-\omega, \mathbf{p}) = -\text{Im } \Sigma(\omega, \mathbf{p}), \quad (3.2)$$

so we restrict ourselves to positive energy  $\omega > 0$ . After suitably relabeling the integration variables, the imaginary part of the self-energy (3.1) for  $\omega > 0$  can be reduced to

$$\text{Im } \Sigma(\omega, \mathbf{p}) = \text{Im } g_1(\omega, \mathbf{p}) + \text{Im } g_2(\omega, \mathbf{p}) \quad (3.3)$$

with the 3-body decay and Landau damping contributions, respectively:

$$\text{Im } g_1(\omega, \mathbf{p}) = \pi(e^{\omega/T} - 1) \int d[k, q] f_k f_q f_r \delta(\omega - E_k - E_q - E_r), \quad (3.4)$$

$$\text{Im } g_2(\omega, \mathbf{p}) = 3\pi(e^{\omega/T} - 1) \int d[k, q] (1 + f_k) f_q f_r \delta(\omega + E_k - E_q - E_r). \quad (3.5)$$

The  $\delta$ -functions in Eqs. (3.4) and (3.5) arise from energy conservation and constrain the integration over  $k$  and  $q$  to the kinematically allowed domain. The evaluation of the resulting kinematic limits of the integration variables is the most demanding part of the following calculation and is shortly discussed in Appendix A. Before going into the technical details of evaluating the integrals, let us summarize some relevant analytical properties of the propagators and self-energies. In the imaginary time formalism, the full propagator

$$D(ip_0, \mathbf{p}) = -\frac{1}{p_0^2 + \mathbf{p}^2 + m_p^2 - \Sigma(ip_0, \mathbf{p})} \quad (3.6)$$

has the spectral representation

$$D(ip_0, \mathbf{p}) = \int_{-\infty}^{\infty} d\omega' \frac{\rho(\omega', \mathbf{p})}{ip_0 - \omega'}. \quad (3.7)$$

The spectral density satisfies

$$\begin{aligned} \rho(\omega, \mathbf{p}) &= -\frac{1}{2\pi i} [D(\omega + i\eta, \mathbf{p}) - D(\omega - i\eta, \mathbf{p})] \\ &= \frac{1}{\pi} \frac{\text{Im } \Sigma(\omega, \mathbf{p})}{[\omega^2 - \mathbf{p}^2 - m_p^2 + \text{Re } \Sigma(\omega, \mathbf{p})]^2 + [\text{Im } \Sigma(\omega, \mathbf{p})]^2}. \end{aligned} \quad (3.8)$$

It is an odd function of  $\omega$ , see Eqs. (3.2):

$$\rho(-\omega, \mathbf{p}) = -\rho(\omega, \mathbf{p}) \quad \text{or} \quad \rho(\omega, \mathbf{p}) = \epsilon(\omega)\rho(|\omega|, \mathbf{p}), \quad (3.9)$$

where  $\epsilon(\omega) = \text{sgn}(\omega)$ . Thus the full propagator  $D(ip_0, \mathbf{p})$  has the following analytical structure: If  $\text{Im } \Sigma \neq 0$ , the full propagator has a cut along the real axis in the complex  $\omega$  plane, with a discontinuity across this cut given by the spectral function. If  $\text{Im } \Sigma$  goes to zero, the identity

$$\frac{1}{\pi} \lim_{\eta \rightarrow 0} \frac{\eta}{A^2 + \eta^2} = \delta(A) \quad (3.10)$$

shows that the spectral density can be expressed as a  $\delta$ -function at  $\omega^2 = \mathbf{p}^2 + m_p^2 - \text{Re } \Sigma(\omega, \mathbf{p})$ ; the corresponding analytical structure of the full propagator  $D(ip_0, \mathbf{p})$  are poles in the complex  $\omega$  plane given by the zeroes of the  $\delta$ -function.

From  $D(ip_0, \mathbf{p})$  the full retarded propagator  $D(\omega + i\eta, \mathbf{p})$  is obtained by analytical continuation  $ip_0 \rightarrow \omega + i\eta$ . The full propagator in the real time formalism can be written as [15]

$$G(\omega, \mathbf{p}) = D(\omega + i\epsilon(\omega)\eta) - 2\pi i \frac{\rho(|\omega|, \mathbf{p})}{e^{|\omega|/T} - 1}. \quad (3.11)$$

All of these full propagators have the same analytical structure.

Defining the damping rate as

$$\gamma(\omega, \mathbf{p}) = \frac{\text{Im } \Sigma(\omega, \mathbf{p})}{2\omega} \quad (3.12)$$

and substituting this into Eq. (3.8), we see that if  $\gamma(\omega, \mathbf{p}) \ll \sqrt{\mathbf{p}^2 + m_p^2 - \text{Re } \Sigma(\omega, \mathbf{p})}$ , then  $\rho(\omega, \mathbf{p})$  is strongly peaked at  $\omega^2 = \mathbf{p}^2 + m_p^2 - \text{Re } \Sigma(\omega, \mathbf{p})$ . The solution of this dispersion relation defines a weakly damped single-particle state which is interpreted as a quasiparticle, the so-called plasmon. Denoting the solution for  $\omega$  by  $\varepsilon(\mathbf{p})$  and defining  $\Gamma \equiv 2\gamma(\varepsilon(\mathbf{p}), \mathbf{p})$ , the spectral density can in this limit be expressed approximately in the form of a relativistic Breit-Wigner function with full width  $\Gamma$ :

$$\rho(\omega, \mathbf{p}) \approx \frac{1}{\pi} \frac{\omega\Gamma}{(\omega^2 - \varepsilon^2(\mathbf{p}))^2 + \omega^2\Gamma^2} \quad (3.13)$$

Finally, the spectral function fulfills the sum rule [16]

$$2 \int_0^\infty d\omega \omega \rho(\omega, \mathbf{p}) = 1. \quad (3.14)$$

In the following two subsections we now investigate in detail the properties of plasmons in  $\phi^4$  theory, both at rest and at finite momentum  $\mathbf{p}$  relative to the heat bath.

### A. Plasmons at rest, $\mathbf{p} = 0$

For  $\mathbf{p} = 0$  the evaluation of the imaginary part of the 2-loop self-energy (3.3) can be carried out in the following manner: for the  $\mathbf{q}$ -integration we choose the  $z$ -axis along  $\mathbf{k}$  and define  $t = \cos(\mathbf{k}, \mathbf{q})$ . The integrals in Eqs. (3.4) and (3.5) thus take the form

$$\pi \int d[k, q] \longrightarrow \frac{g^4}{48(2\pi)^3} \int_0^\infty dk k^2 \int_0^\infty dq q^2 \int_{-1}^1 dt \frac{1}{E_k E_q E_r}, \quad (3.15)$$

where  $E_r = \sqrt{k^2 + q^2 + 2kqt + m_p^2}$ . The energy conserving  $\delta$ -functions in Eqs. (3.4,3.5) will be used to perform the  $t$ -integration by using

$$\frac{dE_r}{dt} = \frac{kq}{E_r}. \quad (3.16)$$

The condition that the zeroes of the  $\delta$ -function fall into the interval  $-1 \leq t \leq 1$ , i.e.  $\sqrt{(k-q)^2 + m_p^2} \leq E_r \leq \sqrt{(k+q)^2 + m_p^2}$ , leads to restrictions of the integration regions in  $k$  and  $q$ . These restrictions are worked out in Appendix A. For the 3-body decay contribution we find

$$\begin{aligned} \text{Im } g_1(\omega, 0) &= \theta(\omega - 3m_p) \frac{g^4 T^2}{384\pi^3} \left( e^{\omega/T} - 1 \right) \\ &\times \int_a^{\varepsilon(x_1^*)} dv f(v) f(w-v) \ln \left( \frac{f(\varepsilon(y_1)) f(\varepsilon(y_2) + v - w)}{f(\varepsilon(y_2)) f(\varepsilon(y_1) + v - w)} \right), \end{aligned} \quad (3.17)$$

where

$$a = \frac{m_p}{T}, \quad w = \frac{\omega}{T}, \quad x = \frac{k}{T}, \quad y = \frac{q}{T}, \quad \varepsilon(z) = \sqrt{z^2 + a^2}, \quad f(v) = \frac{1}{e^v - 1}. \quad (3.18)$$

The specific values  $x_1^*$  and  $y_{1,2}$  are given by Eqs. (A7) and (A4,A5) for  $\mathbf{p} = 0$ , respectively, divided  $T$ .

Similarly, the Landau damping contribution  $\text{Im } g_2(\omega, 0)$  is given by

$$\begin{aligned} \text{Im } g_2(\omega, 0) &= \frac{g^4 T^2}{128\pi^3} \left( e^{\omega/T} - 1 \right) \left[ \theta(m_p - \omega) \int_{\varepsilon(x_4^*)}^{\infty} dv + \theta(\omega - m_p) \int_a^{\infty} dv \right] \\ &\quad \times (1 + f(v)) f(w + v) \ln \left( \frac{f(\varepsilon(y_3)) f(\varepsilon(y_4) - v - w)}{f(\varepsilon(y_4)) f(\varepsilon(y_3) - v - w)} \right), \end{aligned} \quad (3.19)$$

with  $x_4^*$  and  $y_{3,4}$  given by Eqs. (A17) and (A12,A13) for  $\mathbf{p} = 0$ , respectively, divided by  $T$ .

While  $\text{Im } g_1(\omega, 0)$  vanishes below the 3-particle threshold  $E_0^* = 3m_p$  (see Eq. (A2)), the Landau damping contribution  $\text{Im } g_2(\omega, 0)$  (which arises only at  $T \neq 0$ ) is nonzero for *all* positive values of  $\omega$ . Due to the symmetry (3.2), at 2-loop order the full propagator thus has a cut along the whole real  $\omega$  axis. This is qualitatively different from the simple double pole structure at 1-loop order.

On the plasmon mass shell  $\omega = m_p$  only Landau damping contributes to the imaginary part. From Appendix A we find that in this case  $B(m_p, k) = k^2$  and thus  $y_3 = 0$ ,  $y_4 = x$  as well as  $x_4^* = 0$ . Substituting this into Eq. (3.19) and using Eqs. (3.3) and (3.12), we obtain the on-shell plasmon damping rate (see also [12])

$$\gamma(m_p, 0) = \frac{\text{Im } \Sigma(m_p, 0)}{2m_p} = \frac{g^4 T^2}{256\pi^3 m_p} L_2(e^{-a}) = \frac{g^3 T}{64\sqrt{24}\pi} [1 + \mathcal{O}(g \ln g)], \quad (3.20)$$

where  $L_2(z)$  is the Spence function defined as

$$L_2(z) \equiv - \int_0^z dt \frac{\ln(1-t)}{t}. \quad (3.21)$$

The leading term in the last expression of (3.20) was also found in Ref. [11].

$\text{Im } \Sigma$  is finite and does not require any regularization. For dimensional grounds the width  $\gamma(m_p, 0)$  for plasmons at rest is thus proportional to the temperature  $T$ . From (3.20) we further see that for small  $g$  the ratio  $\gamma(m_p, 0)/T$  is proportional to  $g^3$ .

Using Eq. (3.8) we can also evaluate the spectral function. We notice that, as discussed in Section II, the  $\mathcal{O}(g^4)$  term in  $\text{Re } \Sigma$  contains the renormalization scale  $\mu$  which should be absorbed into the renormalized coupling constant. But since the  $\mathcal{O}(g^4)$  corrections have only a minimal effect on the position of the peak in the spectral function, and all  $\mathcal{O}(g^3)$

terms have already been included in the plasmon mass, we can to very good approximation neglect  $\text{Re } \Sigma$ . In this approximation the plasma frequency

$$\omega_p = \varepsilon(\mathbf{p} = 0) = m_p = \frac{gT}{\sqrt{24}} \sqrt{1 - \frac{3g}{\pi\sqrt{24}}} \quad (3.22)$$

is strictly proportional to  $T$ . An additional logarithmic temperature dependence through the running of the coupling constant can only enter in higher order.

In the following we comment on some further properties of the plasmon based on numerical results. In Fig. 4a we show for  $m_{\text{th}}/T = 0.1$  the 2-loop spectral function together with a line indicating the pole position at one-loop order (including HTL resummation). Note that there is no visible shift of the peak due to the higher order corrections; the shift of the peak below the value of  $m_{\text{th}}$  is entirely due to the 1-HTL-resummation, see Eq. (3.22). The major new feature at 2-loop order is just the finite width of the plasmon. Although the 2-loop spectral density is strictly positive for all values of  $\omega$ , it approaches zero very fast as one moves away from the plasmon peak. Only in the neighborhood of the 3-body decay threshold  $\omega = 3m_p$  it gains some weight again as shown in Fig. 4b; the reader should notice, however, the tiny vertical scale of this Figure.

In Fig. 5 we show the plasmon peak in the spectral function for three different values of  $m_{\text{th}}/T = 0.10, 0.11, 0.12$ . Since both the plasmon frequency and its width grow linearly with  $T$ , and according to Eq. (3.13)  $\rho(\omega_p) \approx 1/(\pi\omega_p\Gamma)$ , the height of the peak decreases with rising temperature like  $1/T^2$  for fixed  $g$ . This is seen in Fig. 5.  $T^2\rho(\omega_p)$  decreases accordingly with increasing coupling constant like  $1/g^4$  for small  $g$ .

For small  $g$  the ratio of the damping rate to the plasma frequency is

$$\frac{\gamma(m_p, 0)}{\omega_p} \approx \frac{g^2}{64\pi}. \quad (3.23)$$

From Eq. (3.22) we see that our resummation procedure is only applicable for  $\lambda = \frac{g^2}{24} < \frac{\pi^2}{9} \simeq 1$ . In this domain the ratio (3.23) is always smaller than about 1/10, i.e. the plasmon is a well-defined quasiparticle which is not overdamped.

## B. Moving Plasmons, $\mathbf{p} \neq 0$

The evaluation of the imaginary part of the self-energy for  $\mathbf{p} \neq 0$  is a little more complicated because now two non-trivial angular integrations occur. For the  $q$ -integration we choose the  $z$ -axis in the direction of  $\mathbf{k} - \mathbf{p}$  and define  $t = \cos(\mathbf{k} - \mathbf{p}, \mathbf{q})$ . For the  $k$ -integration we choose the  $z$ -axis along  $\mathbf{p}$  and define  $u = \cos(\mathbf{p}, \mathbf{k})$ . In this way the integrals in Eqs. (3.4) and (3.5) can be expressed as

$$\pi \int d[k, q] \longrightarrow \frac{g^4}{96(2\pi)^3} \int_0^\infty dk k^2 \int_{-1}^1 du \int_0^\infty dq q^2 \int_{-1}^1 dt \frac{1}{E_k E_q E_r}. \quad (3.24)$$

The occurrence of two angles in the integrand renders the determination of the integration limits from the energy-conserving  $\delta$ -functions more complicated. However, as shown in Appendix A, similar methods can be applied as in the case  $\mathbf{p} = 0$ . The  $t$ -integration in Eq. (3.24) can be performed by using

$$\frac{dE_r}{dt} = \frac{q|\mathbf{k} - \mathbf{p}|}{E_r}. \quad (3.25)$$

The condition that the zero of the energy  $\delta$ -function lies inside integration domain leads to kinematic limits for the integrations over  $q$ ,  $k$ , and  $u$ . We find (see Appendix A)

$$\begin{aligned} \text{Im } g_1(\omega, \mathbf{p}) = & \theta(\omega - E_p^*) \frac{g^4 T^2}{768\pi^3} (e^{\omega/T} - 1) \int_{-1}^1 du \int_0^{x_1^*} \frac{dx x^2}{|\mathbf{x} - \mathbf{z}| \varepsilon(x)} \\ & \times f(\varepsilon(x)) f(w - \varepsilon(x)) \ln \left( \frac{f(\varepsilon(y_1)) f(\varepsilon(y_2) + \varepsilon(x) - w)}{f(\varepsilon(y_2)) f(\varepsilon(y_1) + \varepsilon(x) - w)} \right) \end{aligned} \quad (3.26)$$

with the same dimensionless variables (3.18) as before and

$$\mathbf{z} = \frac{\mathbf{p}}{T}. \quad (3.27)$$

The limits  $x_1^*$ ,  $y_1$ , and  $y_2$  are now given by Eqs. (A6), (A4), and (A5), respectively, divided by  $T$ . In the limit  $\mathbf{p} \rightarrow 0$  ( $z \rightarrow 0$ ) Eq. (3.26) correctly reduces to Eq. (3.17).

For the Landau damping contribution  $\text{Im } g_2(\omega, \mathbf{p})$  we obtain

$$\begin{aligned} \text{Im } g_2(\omega, \mathbf{p}) = & \frac{g^4 T^2}{256\pi^3} (e^{\omega/T} - 1) \int d(u, x) (1 + f(\varepsilon(x))) f(w + \varepsilon(x)) \\ & \times \ln \left( \frac{f(\varepsilon(y_3)) f(\varepsilon(y_4) - \varepsilon(x) - w)}{f(\varepsilon(y_4)) f(\varepsilon(y_3) - \varepsilon(x) - w)} \right), \end{aligned} \quad (3.28)$$

where

$$\begin{aligned}
\int d(u, x) \equiv & \\
& \theta(E_p - \omega) \left[ \theta(\tilde{E}_p - \omega) \left( \theta(p - \omega) \int_{-\omega/p}^1 du + \theta(\omega - p) \int_{-1}^1 du \right) \int_{x_4^*}^{\infty} dx \right. \\
& \left. + \theta(\omega - \tilde{E}_p) \left( \int_{-1}^{u^*} du \int_{x_4^*}^{\infty} dx + \int_{u^*}^1 du \int_0^{\infty} dx \right) \right] \frac{x^2}{|\mathbf{x} - \mathbf{z}| \varepsilon(x)} \\
& + \theta(\omega - E_p) \frac{1}{z} \int_a^{\infty} d\varepsilon(x) \int_{|x-z|}^{|x+z|} d|\mathbf{x} - \mathbf{z}| \tag{3.29}
\end{aligned}$$

if  $p < 3m_p/2$  and

$$\begin{aligned}
\int d(u, x) \equiv & \\
& \theta(E_p - \omega) \left[ \theta(\tilde{E}_p - \omega) \int_{-\omega/p}^1 du \int_{x_4^*}^{\infty} dx \right. \\
& \left. + \theta(\omega - \tilde{E}_p) \left( \theta(p - \omega) \left( \int_{-\omega/p}^{u^*} du \int_{x_4^*}^{\infty} dx + \int_{u^*}^1 du \int_0^{\infty} dx \right) \right. \right. \\
& \left. \left. + \theta(\omega - p) \left( \int_{-1}^{u^*} du \int_{x_4^*}^{\infty} dx + \int_{u^*}^1 du \int_0^{\infty} dx \right) \right) \right] \frac{x^2}{|\mathbf{x} - \mathbf{z}| \varepsilon(x)} \\
& + \theta(\omega - E_p) \frac{1}{z} \int_a^{\infty} d\varepsilon(x) \int_{|x-z|}^{|x+z|} d|\mathbf{x} - \mathbf{z}| \tag{3.30}
\end{aligned}$$

if  $p > 3m_p/2$ , respectively. In deriving these expressions from the results (A19) and (A20) in Appendix A, we used for the region  $\omega > E_p$  the relation

$$\frac{d|\mathbf{k} - \mathbf{p}|}{du} = -\frac{k p}{|\mathbf{k} - \mathbf{p}|} \tag{3.31}$$

to rewrite the  $u$ -integration. Since the integrand in (3.28) does not depend on  $u$ , the resulting integrals  $\int d|\mathbf{x} - \mathbf{z}|$  in (3.29) and (3.30) can be evaluated trivially. Again  $\text{Im } g_2(\omega, \mathbf{p})$  is non-zero for all  $\omega > 0$ , and the full propagator has a cut along the whole real  $\omega$  axis, arising from Landau damping as for the case  $\mathbf{p} = 0$ . One easily checks that in the zero-momentum limit Eq. (3.28) reduces to (3.19).

On the plasmon energy shell  $\omega = \sqrt{\mathbf{p}^2 + m_p^2}$  the plasmon damping rate can be deduced

as

$$\begin{aligned}
\gamma(\sqrt{\mathbf{p}^2 + m_p^2}, \mathbf{p}) = & \frac{g^4 T}{256 \pi^3} \frac{1}{z \varepsilon(z)} \int_0^z dx \left[ L_2(\xi) + L_2 \left( \frac{\xi - \zeta}{\xi(1 - \zeta)} \right) \right. \\
& \left. - L_2 \left( \frac{\xi - \zeta}{1 - \zeta} \right) - L_2 \left( \frac{(\xi - \zeta)(1 - \xi\zeta)}{\xi(1 - \zeta)^2} \right) \right], \tag{3.32}
\end{aligned}$$

where

$$\xi = e^{-\sqrt{z^2+a^2}}, \quad \zeta = e^{-\sqrt{x^2+a^2}}. \quad (3.33)$$

This on-shell result has also recently been obtained by Jeon [12] by a different method.

For the numerical evaluation of the spectral function we substitute Eqs. (3.26) and (3.28) into Eq. (3.3) and then use Eq. (3.8). In Fig. 6 we show the spectral density at fixed  $m_{\text{th}}/T = 0.1$  for three values of the momentum  $p/T$ . As  $p/T$  increases, the width of the spectral function decreases as illustrated in Fig. 7. For large  $p/T$  the width goes to zero, and at the same time the height of the spectral function approaches a constant. This can be seen explicitly in Figs. 7 and 8. This means that for large  $p/T$  the plasmon loses the features of a collective mode and again behaves like a non-interacting free particle! At fixed, non-zero momentum  $\mathbf{p}$  the dependences on the temperature  $T$  and the coupling constant  $g$ , on the other hand, are qualitatively the same as at  $\mathbf{p} = 0$ .

From the analysis of HTL resummation in gauge theories [6] it is known that there the summation scheme can only be guaranteed to work in the soft momentum region  $\omega, p \sim gT < T$ . A partial reason for this is that the thermal loops are momentum dependent, and the particular momentum dependence of the “hard” thermal loop arises as the leading term in a high-temperature expansion of the 1-loop self energy [1]. Correspondingly, one might be inclined to distrust the above results for momenta  $p/T \gg 1$ . In  $\phi^4$  theory the situation is, however, different in that the HTL which we resum is momentum independent to order  $g^2$  and  $g^3$ ; momentum dependence enters only at order  $g^4$ , and for weak coupling  $\lambda = \frac{g^2}{24} \ll 1$  as in Figs. 6, 7 it is weak on the scale  $m_p$ . Therefore the essential criterium for the validity of the resummation procedure is the smallness of the coupling constant and not that of  $\omega/T$  or  $p/T$ .

This argument is also supported by a numerical investigation of the sum rule Eq. (3.14). In Table I we give values for the integral up to the 3-particle threshold,

$$I_{\text{sum}} = 2 \int_0^{E_p^*} d\omega \omega \rho(\omega, \mathbf{p}), \quad (3.34)$$

for different values of  $m_{\text{th}}/T$  (or of the coupling constant  $\lambda = g^2/24$ ) at  $\mathbf{p} = 0$  and for different values of  $p/T$  at fixed  $m_{\text{th}}/T = 0.1$ . From the given numbers we see that in all cases the sum rule is nearly exhausted by the collective plasmon mode, and that the 3-body decay contribution at  $\omega > E_p^*$  is negligible. For large coupling constant ( $m_{\text{th}}/T > 1$ ), where the resummation of hard thermal loops is no longer expected to be a good approximation, we begin to see appreciable violations of the sum rule. On the other hand, for  $m_{\text{th}}/T = 0.1$ , the sum rule is very well satisfied even for very large momenta,  $p/T \simeq 100$ . As a consequence, the shape of the spectral function (in particular the interplay of the  $p$ -dependence of its width and height at the plasmon pole shown in Figs. 7 and 8) is completely controlled by this sum rule.

#### IV. CONCLUSIONS

In this paper we studied the analytical structure of the full propagator and the properties of the plasmon in hot  $\phi^4$  theory at 2-loop order, using the hard thermal loop (HTL) resummation scheme.

Since in  $\phi^4$  theory the one-loop self-energy is completely real, damping of the plasmon occurs only at the 2-loop level. Its physical origin is Landau damping by scattering with thermal scalar field quanta. This results in a cut of the full propagator along the entire real frequency axis. However, for small coupling constant  $g$  the spectral function which is given by the discontinuity across this cut shows a strong and rather sharp plasmon peak located at the position expected from the 1-HTL-resummation. Its width  $\Gamma/\omega_p$  is approximately given by  $g^2/(32\pi)$  for plasmons at rest in the heat bath, and this width decreases even further if the plasmon is moving relative to the heat bath. For very fast plasmons the width goes to zero while the height of the plasmon peak approaches to a constant: the plasmon behaves again like a non-interacting free particle, i.e. it loses the features of a collective mode. Within the range of validity of our resummation scheme, which is defined by the smallness of the coupling constant  $\lambda = \frac{g^2}{24}$  compared to 1, the plasmon remains a well-defined, weakly-

damped quasiparticle excitation for all values of the temperature. The sum rule Eq. (3.14) for the spectral density is very well satisfied by the 2-loop result even for momenta much larger than  $T$ , and it is essentially saturated by the plasmon peak.

## ACKNOWLEDGMENTS

We are grateful to U. Wiedemann for helpful discussions, and we would like to thank the referee for a careful reading of the manuscript and for pointing out an error in the original version of the paper. This work was supported in part by the Deutsche Forschungsgemeinschaft (DFG), the Bundesministerium für Bildung und Forschung (BMBF), the National Natural Science Foundation of China (NSFC) and the Gesellschaft für Schwerionenforschung (GSI).

## APPENDIX A: KINEMATIC LIMITS FOR THE COLLISION INTEGRALS

Here we give some technical details on how to solve for the kinematic limits of the integral (3.24) resulting from the energy conserving  $\delta$ -functions. We perform the calculation for arbitrary external momentum  $\mathbf{p}$ ; the expressions needed in Section III A for plasmons at rest are easily obtained by setting  $\mathbf{p} = 0$ . In this limit the integrand is independent of  $u$ , and the  $u$ -integration gives a trivial factor of 2.

We start by doing the  $t$ -integration in (3.24) using (3.25) and exploiting the energy  $\delta$ -function. In order to obtain a non-zero contribution, the solution  $E_r$  of the  $\delta$ -function constraint must lie in the interval

$$\sqrt{(|\mathbf{k} - \mathbf{p}| - q)^2 + m_p^2} \leq E_r \leq \sqrt{(|\mathbf{k} - \mathbf{p}| + q)^2 + m_p^2} \quad (\text{A1})$$

defined by the limits of the  $t$  integration,  $-1 \leq t \leq 1$ . For fixed  $|\mathbf{k} - \mathbf{p}|$  (or fixed  $k$  and  $u$ ) these limits on  $E_r$  generate upper and lower integration limits for  $q$ . If the latter are complex, the corresponding values of  $k$  and  $u$  must be excluded from the exterior integrations.

For the 3-body decay (3.4) we must solve  $\omega - E_k - E_q - E_r = 0$ , with the notation of Eqs. (2.12), (2.13). This has no solutions unless  $\omega$  exceeds the 3-particle threshold

$$E_p^* = m_p + \sqrt{p^2 + 4m_p^2}. \quad (\text{A2})$$

With the help of the auxiliary function

$$A(\omega, |\mathbf{k} - \mathbf{p}|) = \frac{(\omega - E_k)^2 ((\omega - E_k)^2 - (\mathbf{k} - \mathbf{p})^2 - 4m_p^2)}{(\omega - E_k)^2 - (\mathbf{k} - \mathbf{p})^2} \quad (\text{A3})$$

the lower and upper integration limits for  $q$  which result from (A1) can be expressed as

$$q_1 = \max[0, q'_1] \quad \text{with} \quad q'_1 = \frac{1}{2} \left( \sqrt{A(\omega, |\mathbf{k} - \mathbf{p}|)} - |\mathbf{k} - \mathbf{p}| \right) \quad (\text{A4})$$

and

$$q_2 = \frac{1}{2} \left( \sqrt{A(\omega, |\mathbf{k} - \mathbf{p}|)} + |\mathbf{k} - \mathbf{p}| \right). \quad (\text{A5})$$

For  $q_1, q_2$  to be real,  $A(\omega, |\mathbf{k} - \mathbf{p}|)$  must be positive. The function  $A$  is shown in Fig. 3a.  $A(\omega, |\mathbf{k} - \mathbf{p}|)$  has a single zero at

$$k_1^* = \frac{pu(\omega^2 - p^2 - 3m_p^2) + \omega\sqrt{(\omega^2 - p^2 - 3m_p^2)^2 - 4(\omega^2 - p^2u^2)m_p^2}}{2(\omega^2 - p^2u^2)}, \quad (\text{A6})$$

which for  $\mathbf{p} = 0$  reduces to

$$k_1^* = \frac{\sqrt{(\omega^2 - m_p^2)(\omega^2 - 9m_p^2)}}{2\omega}, \quad (\text{A7})$$

a  $\mathbf{p}$ -independent double zero at

$$k_3^* = \sqrt{\omega^2 - m_p^2}, \quad (\text{A8})$$

and a singularity in between at

$$k_2^* = \frac{pu(\omega^2 - p^2 + m_p^2) + \omega\sqrt{(\omega^2 - p^2 + m_p^2)^2 - 4(\omega^2 - p^2u^2)m_p^2}}{2(\omega^2 - p^2u^2)}, \quad (\text{A9})$$

which for  $\mathbf{p} = 0$  becomes simply

$$k_2^* = \frac{\omega^2 - m_p^2}{2\omega}. \quad (\text{A10})$$

One checks that for  $k > k_2^*$  the energy constraint cannot be satisfied; for  $k_1^* < k < k_2^*$  the function  $A(\omega, |\mathbf{k} - \mathbf{p}|)$  is negative, giving rise to complex  $q$  integration limits. Hence the

allowed region for  $k$  is  $0 \leq k \leq k_1^*$ . There is no constraint on  $u$ . The  $q$ -integration can be done analytically, giving the results presented in Section III.

For the Landau damping term (3.5) the calculation is slightly more involved. We must solve  $\omega - E_k - E_q - E_r = 0$  with the restriction (A1). For fixed  $|\mathbf{k} - \mathbf{p}|$  the resulting lower and upper limits for  $q$  can now be expressed in terms of another auxiliary function

$$B(\omega, |\mathbf{k} - \mathbf{p}|) = \frac{(\omega + E_k)^2 ((\omega + E_k)^2 - (\mathbf{k} - \mathbf{p})^2 - 4m_p^2)}{(\omega + E_k)^2 - (\mathbf{k} - \mathbf{p})^2} \quad (\text{A11})$$

as

$$q_3 = \max[0, q'_3] \quad \text{with} \quad q'_3 = \frac{1}{2} \left( \sqrt{B(\omega, |\mathbf{k} - \mathbf{p}|)} - |\mathbf{k} - \mathbf{p}| \right), \quad (\text{A12})$$

and

$$q_4 = \frac{1}{2} \left( \sqrt{B(\omega, |\mathbf{k} - \mathbf{p}|)} + |\mathbf{k} - \mathbf{p}| \right). \quad (\text{A13})$$

The function  $B(\omega, k)$  is illustrated in Fig. 3b. For  $\omega \geq E_p$ ,  $B(\omega, |\mathbf{k} - \mathbf{p}|)$  is always positive, so  $q_3, q_4$  are real and the  $\delta$ -function can be satisfied for all  $k \in [0, \infty]$  and  $u \in [-1, 1]$ . For  $\omega < E_p$ ,  $B(\omega, |\mathbf{k} - \mathbf{p}|)$  has a positive and real zero at

$$k_4^* = \frac{pu(\omega^2 - p^2 - 3m_p^2) + \omega\sqrt{(\omega^2 - p^2 - 3m_p^2)^2 - 4(\omega^2 - p^2u^2)m_p^2}}{2(\omega^2 - p^2u^2)}. \quad (\text{A14})$$

if simultaneously  $u < u^*$  with

$$u^* = -\frac{\sqrt{4\omega^2 m_p^2 - (\omega^2 - p^2 - 3m_p^2)^2}}{2p m_p}. \quad (\text{A15})$$

$u^*$  itself is real only for  $\omega \geq \tilde{E}_p$  where

$$\tilde{E}_p = \sqrt{p^2 + 4m_p^2} - m_p. \quad (\text{A16})$$

For  $\tilde{E}_p < \omega < E_p$ , positivity of  $B(\omega, |\mathbf{k} - \mathbf{p}|)$  thus restricts the integration range of  $k$  to  $k > k_4^*$  if  $u < u^*$ , while all  $k$  are allowed for  $u > u^*$ . For  $\omega < \tilde{E}_p$  there is no upper constraint on  $u$ , and  $k$  is restricted to the region  $k > k_4^*$ .

For  $\mathbf{p} = 0$ , there is no constraint on  $u$ , and  $k_4^*$  reduces to

$$k_4^* = \frac{\sqrt{(m_p^2 - \omega^2)(9m_p^2 - \omega^2)}}{2\omega}. \quad (\text{A17})$$

We can summarize the results so far by writing

$$\begin{aligned} \int du \int dk \longrightarrow & \theta(E_p - \omega) \left[ \theta(\tilde{E}_p - \omega) \int_{k_4^*}^1 du \int_{k_4^*}^{\infty} dk \right. \\ & + \theta(\omega - \tilde{E}_p) \left( \int_{k_4^*}^{u^*} du \int_{k_4^*}^{\infty} dk + \int_{u^*}^1 du \int_0^{\infty} dk \right) \left. \right] \\ & + \theta(\omega - E_p) \int_{-1}^1 du \int_0^{\infty} dk. \end{aligned} \quad (\text{A18})$$

The missing *lower* limits of the  $u$ -integration in two of the terms will be determined now.

Eq. (A14) shows that for  $\omega < p$ ,  $k_4^*$  has a singularity at  $u = -\omega/p$ . (At  $u = +\omega/p$ ,  $k_4^*$  remains finite because the numerator vanishes, too.) This implies an additional restriction on the lower limit of the  $u$  integration domain for the two  $k_4^*$ -dependent terms in Eq. (A18) whenever  $\omega < p$ . Which of these two terms is affected depends on the magnitude of  $p$ : For  $p < 3m_p/2$  we find also  $p < \tilde{E}_p$ , so in this case the second term in Eq. (A18) is not affected by this problem because it receives contributions only from  $\omega > \tilde{E}_p > p$ . For  $p > 3m_p/2$  we get also  $p > \tilde{E}_p$ , and then both the first and the second term in Eq. (A18) are affected. It turns out that the region  $u < -\omega/p$  is always unphysical because either the function  $B$  is negative or the  $\delta$ -function constraint cannot be satisfied. One thus finds, using the dimensionless quantities (3.18),

$$\begin{aligned} \int du \int dk & \xrightarrow{p < 3m_p/2} \\ & \theta(E_p - \omega) \left[ \theta(\tilde{E}_p - \omega) \left( \theta(p - \omega) \int_{-\omega/p}^1 du + \theta(\omega - p) \int_{-1}^1 du \right) \int_{x_4^*}^{\infty} dx \right. \\ & + \theta(\omega - \tilde{E}_p) \left( \int_{-1}^{u^*} du \int_{x_4^*}^{\infty} dx + \int_{u^*}^1 du \int_0^{\infty} dx \right) \left. \right] \\ & + \theta(\omega - E_p) \int_{-1}^1 du \int_0^{\infty} dx \end{aligned} \quad (\text{A19})$$

and

$$\begin{aligned} \int du \int dk & \xrightarrow{p > 3m_p/2} \\ & \theta(E_p - \omega) \left[ \theta(\tilde{E}_p - \omega) \int_{-\omega/p}^1 du \int_{x_4^*}^{\infty} dx \right. \end{aligned}$$

$$\begin{aligned}
& + \theta(\omega - \tilde{E}_p) \left( \theta(p - \omega) \left( \int_{-\omega/p}^{u^*} du \int_{x_4^*}^{\infty} dx + \int_{u^*}^1 du \int_0^{\infty} dx \right) \right. \\
& \quad \left. + \theta(\omega - p) \left( \int_{-1}^{u^*} du \int_{x_4^*}^{\infty} dx + \int_{u^*}^1 du \int_0^{\infty} dx \right) \right) \Big] \\
& + \theta(\omega - E_p) \int_{-1}^1 du \int_0^{\infty} dx .
\end{aligned} \tag{A20}$$

## REFERENCES

\* On leave of absence from Hua-Zhong Normal University, Wuhan, China

- [1] H. A. Weldon, Phys. Rev. D**26**, 1394 (1982); V. V. Klimov, Sov. J. Nucl. Phys. **33**, 934 (1981).
- [2] U. Heinz and P. J. Siemens, Phys. Lett. B**158**, 11 (1985).
- [3] H. A. Weldon, Phys. Rev. D**26**, 2789 (1982); and Phys. Rev. D**40**, 2410 (1989).
- [4] E. Braaten and R. D. Pisarski, Phys. Rev. D**46**, 1829 (1992).
- [5] J.I. Kapusta, *Finite Temperature Field Theory* (Cambridge University Press, Cambridge, 1989).
- [6] R. D. Pisarski, Phys. Rev. Lett. **63**, 1129 (1989); E. Braaten and R. D. Pisarski, Nucl. Phys. B**337**, 569 (1990).
- [7] A. Hosoya, M.-A. Sakagami and M. Takao, Ann. Phys. (N.Y.) **154**, 229 (1984).
- [8] S. Jeon, Phys. Rev. D**47**, 4586 (1993).
- [9] D. N. Zubarev, *Nonequilibrium Statistical Thermodynamics*, (Plenum, New York, 1974).
- [10] L. Dolan and R. Jackiw, Phys Rev. D**9**, 3320 (1974).
- [11] R. R. Parwani, Phys. Rev. D**45**, 4695 (1992).
- [12] S. Jeon, *Hydrodynamic Transport Coefficients in Relativistic Scalar Field Theory*, University of Washington preprint, UW/PT 94-09, unpublished.
- [13] S. V. Ilyin, A. D. Panferov, and Yu. M. Sinyukov, Phys. Lett. B**227**, 455 (1989).
- [14] R. D. Pisarski, Nucl. Phys. B**309**, 476 (1988).
- [15] H. A. Weldon, Phys. Rev. D**28**, 2007 (1983).

[16] R. D. Pisarski, Physica A**158**, 146 (1989).

## FIGURES

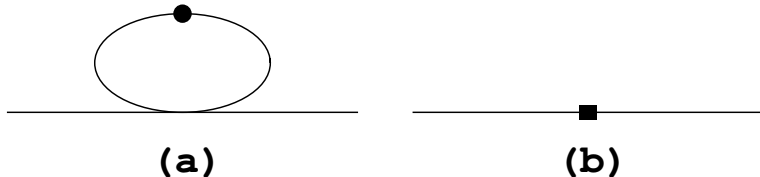


FIG. 1. Lowest order contributions to the self energy for the resummed effective Lagrangian. Lines with a dot denote effective propagators with masses  $m_{\text{th}}$  or  $m_p$ , respectively. The squared box denotes the additional interaction due to the mass shift.

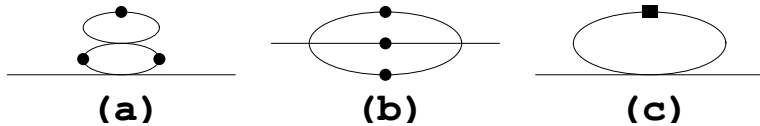


FIG. 2. Next-to-lowest-order contributions to the self energy for the resummed effective Lagrangian.

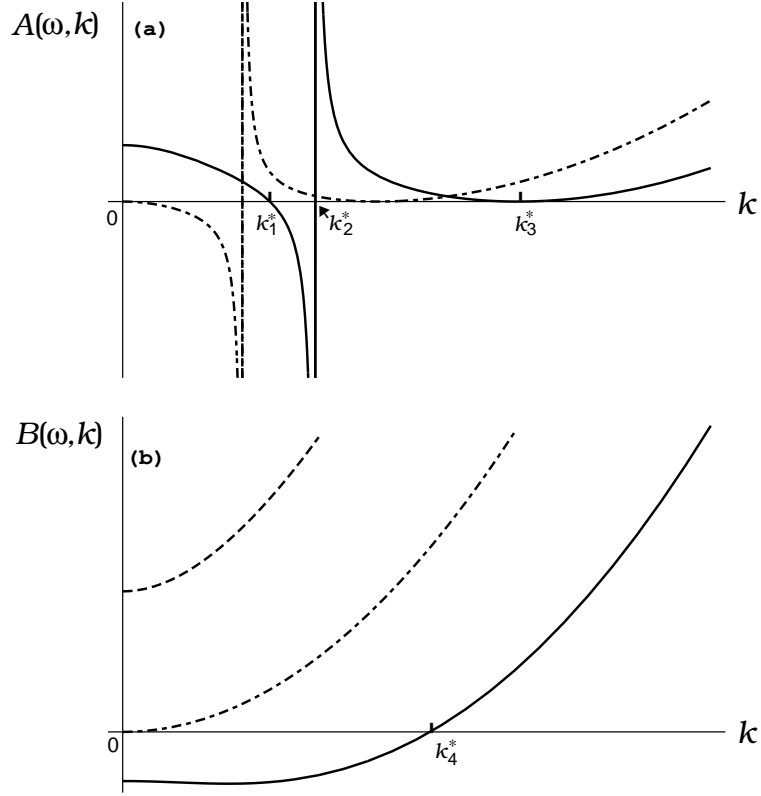


FIG. 3. (a) The function  $A(\omega, k)$  vs.  $k$  for  $\omega > 3m_p$  (solid line) and for  $\omega = 3m_p$  (dot-dashed line);  $k_1^*$  and  $k_3^*$  indicate the two zeroes and  $k_2^*$  the singularity of the solid curve. (b) The function  $B(\omega, k)$  vs.  $k$  for  $\omega < m_p$  (solid line), for  $\omega = m_p$  (dot-dashed line) and for  $\omega > m_p$  (dashed line);  $k_4^*$  indicates the zero of the solid curve.

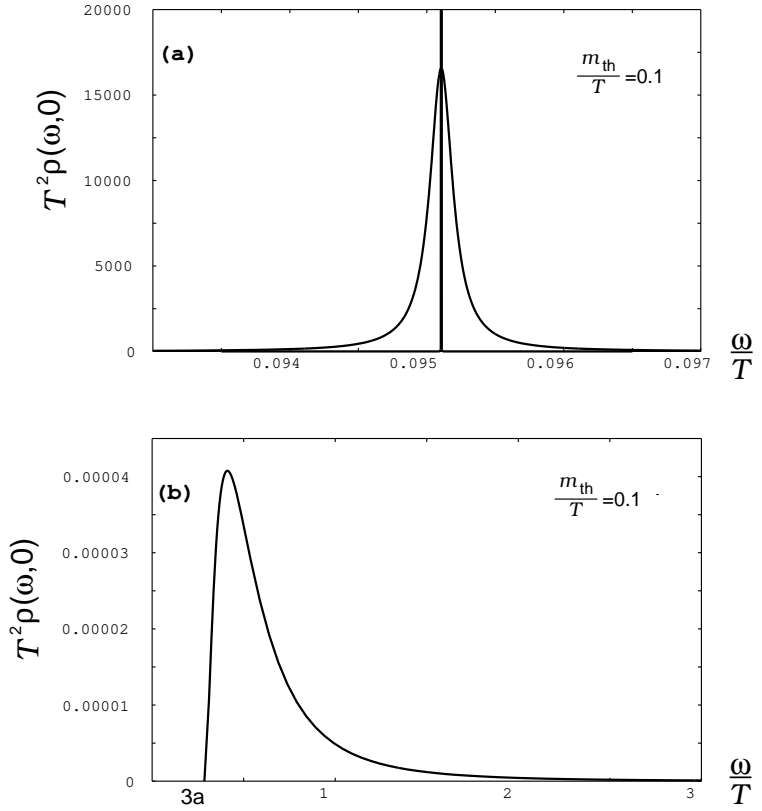


FIG. 4. The two-loop spectral function for  $m_{\text{th}}/T = 0.1$ . The vertical line at the peak position in the upper diagram indicates the spectral  $\delta$ -function at one-loop order.

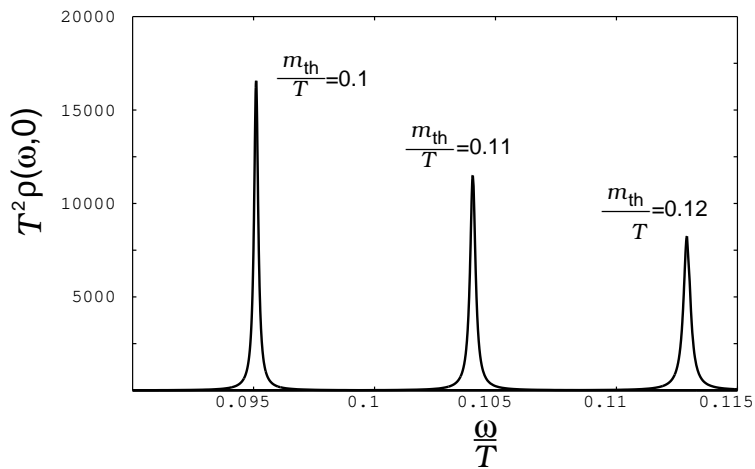


FIG. 5. The two-loop spectral function for different values of  $m_{\text{th}}/T$  (or coupling constant  $g$ ).

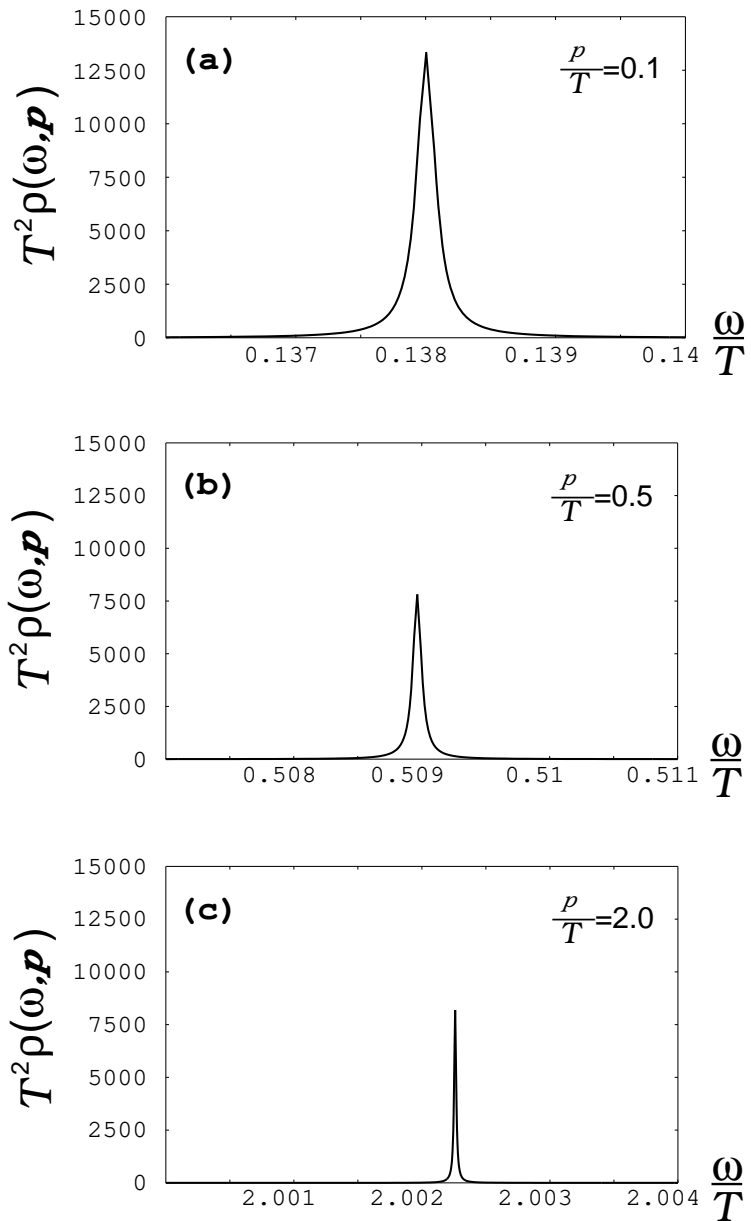


FIG. 6. The two-loop spectral density at fixed  $m_{\text{th}}/T = 0.1$  for different values of  $p/T$ .

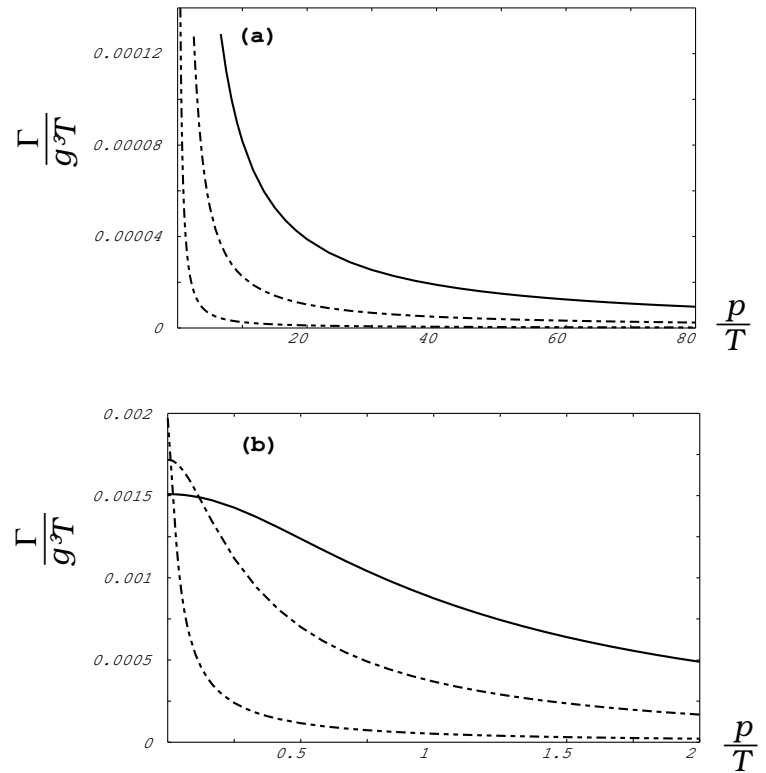


FIG. 7. (a) The width of the spectral function vs.  $p/T$  for  $m_{\text{th}}/T = 0.01$  (dot-dashed line),  $m_{\text{th}}/T = 0.1$  (dashed line) and  $m_{\text{th}}/T = 0.5$  (solid line). (b) Close-up of (a) for small  $p/T$ .

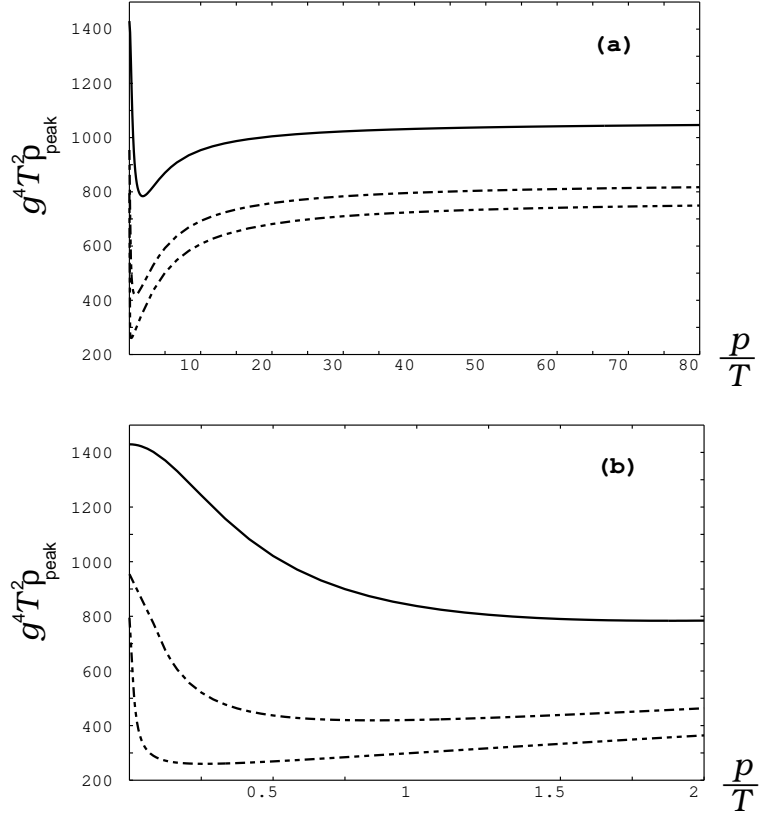


FIG. 8. (a) The peak value of the spectral function vs.  $p/T$  for  $m_{\text{th}}/T = 0.01$  (dot-dashed line) and  $m_{\text{p}}/T = 0.1$  (dashed line) and  $m_{\text{th}}/T = 0.5$  (solid line). (b) Close-up of (a) for small  $p/T$ .

## TABLES

TABLE I. The values of  $I_{\text{sum}}$  for different values of  $m_{\text{th}}/T$  at fixed  $\mathbf{p}=0$  (upper half) and for different values of  $p/T$  at fixed  $m_{\text{th}}/T = 0.1$  (lower half).

$m_{\text{th}}/T$	0.05	0.1	0.5	1.0
$I_{\text{sum}}$	0.9834	0.9852	0.9916	1.0669
$p/T$	0.	10.	20.	80.
$I_{\text{sum}}$	0.9852	0.9896	0.9903	0.9914